Improved Direct Bioelectrochemical Fructose Oxidation with Surfactant-Free Heterotrimeric Fructose Dehydrogenase Variant Truncating Heme 1*c* and C-Terminal Hydrophobic Regions

Taiki Adachi[a], Konatsu Ichikawa[a], Tomoko Miyata[b], Fumiaki Makino[b,c], Hideaki Tanaka[d], Keiichi Namba[b,e,f], Keisei Sowa[a]*

a) Division of Applied Life Sciences, Graduate School of Agriculture, Kyoto University, Sakyo, Kyoto 606-8502, Japan

b) Graduate School of Frontier Biosciences, Osaka University, Suita, Osaka 565-0871, Japan

c) JEOL Ltd., Akishima, Tokyo 196-8558, Japan

d) TechnoPro R&D Company, Kobe, Hyogo 650-0047, Japan

e) RIKEN Center for Biosystems Dynamics Research, Suita, Osaka 565-0874, Japan

f) RIKEN SPring-8 Center, Sayo, Hyogo 679-5198, Japan

KEYWORDS: Bioelectrocatalysis, Direct electron transfer, Fructose dehydrogenase, Surfactant-free solubilization, Cryo-electron microscopy

ABSTRACT: Direct electron transfer (DET)-type bioelectrocatalysis is a coupled redox reaction between enzymatic and electrode reactions. Such mediatorless reactions are an environmentally safe approach that can be applied to various bioelectrochemical devices. We focused on fructose dehydrogenase (FDH), a membrane-bound heterotrimeric enzyme that catalyzes DET-type D-fructose oxidation. Although the overall structure was recently elucidated, its membrane-bound region has not been completely identified. Therefore, this study assumed that the heme 1*c* region and C-terminal hydrophobic region (CHR) were bound to the membrane. A constructed double variant (Δ1*c*ΔCHR_FDH) was soluble without any surfactants; additionally, cryo-electron microscopy confirmed that this variant was downsized. Δ1*c*ΔCHR_FDH exhibited a 14-fold higher catalytic current density (11 ± 1 mA cm^{-2}) than that of the wild-type recombinant FDH (rFDH) at multi-walled carbon nanotube electrodes. Kinetic analysis of the voltammograms suggested that downsizing of the enzyme and the removal of surfactants increased the surface concentration of enzymes at the electrode. This study elucidates the membrane-binding mechanism of proteins and efficient bioelectrocatalysis overcoming the interference of surfactants.

1. INTRODUCTION

Enzymes are useful catalysts that exhibit high activity and selectivity under mild conditions (normal temperature, normal pressure, and neutral pH). Oxidoreductases—the largest class of enzymes—participate in biochemical electron transfer reactions, such as respiration, photosynthesis, and fermentation, in all living organisms. Therefore, the disadvantages observed using organic, inorganic, and metallic catalysts can be addressed by using oxidoreductases to conduct numerous green chemical reactions. Some oxidoreductases exhibit low selectivity for one of the two substrates (an electron donor or acceptor), which can be replaced with conductive electrode materials. The enzyme can proceed with substrate conversion on the electrode using electrical energy without additional redox mediators. This coupled reaction is called direct electron transfer (DET)-type bioelectrocatalysis,[1–6] and has been used as a kinetically and thermodynamically simple analytical method for the implementation of enzymes in applications such as biosensors,[7–16] biofuel cells,[16–22] biosupercapacitors,[23] and bioelectrosynthesis.[24–28]

Nanostructured electrode materials have been widely used for enhancing DET-type bioelectrocatalysis.[29–34] The nanostructure contributes to: 1) the enlargement of the effective electrode area for enzyme adsorption, 2) increase in the probability that the enzymatic electrode-active site faces the surface of the electrode because of the curvature of the pores of the electrode,[35,36] and 3) acceleration of heterogeneous electron transfer at the edge of electrode pores owing to the strengthened electric field.[37]

The effects of surfactants must be considered in DET-type bioelectrocatalysis using membrane enzymes. Surfactants are required for the purification and stabilization of membrane enzymes. However, surfactants can impede enzyme adsorption on the surface of the electrode.[38] Therefore, removing surfactants from the enzymatic mixture may improve DET-type bioelectrocatalysis.

The membrane-bound fructose dehydrogenase (FDH) from *Gluconobacter japonicus* NBRC3260 is a representative DET-type enzyme that catalyzes the oxidation of D-fructose to 5-keto-D-fructose.[39] Because of its high activity and substrate specificity, FDH has been used as a bioelectrocatalyst on DET-based fructose biosensors[40–52] and fructose/O_2 biofuel cells.[53–55] FDH is a 130-kDa heterotrimer comprising a large catalytic subunit (subunit L; 60 kDa), a small chaperone-like subunit (subunit S; 17 kDa), and a membrane-bound cytochrome *c* subunit (subunit C; 49 kDa). Subunit L contains a covalently bound flavin adenine dinucleotide (FAD) and an iron-sulfur cluster ([3Fe-4S]), whereas subunit C has three hemes *c* —1*c*, 2*c*, and 3*c*—from N-terminus. FDH physiologically works in the respiratory chain, and the electrons extracted from D-fructose are finally transferred to ubiquinone-10 (UQ_{10}) via FAD, [3Fe-4S], heme 3*c*, heme 2*c*, and heme 1*c* in this order.[56] In contrast, electrode materials are accessible to heme 2*c* in the DET-type reaction.[57] Therefore, DET-type reactions do not require heme 1*c*. An FDH variant deleting the heme 1*c* region (Δ1*c*_FDH) exhibited a higher DET-type current density than that of the wild-type recombinant FDH (rFDH) owing to an increase in the amount of the downsized enzyme at the surface of the electrode.[58]

The heterotrimeric structure of FDH is conserved among DET-type respiratory chain dehydrogenases of acetic acid bacteria, such as alcohol, aldehyde, and gluconate dehydrogenases.[59–62] The glucose dehydrogenase from *Burkholderia cepacia* exhibited high similarity to FDH.[63] FDH contains a membrane-bound helix at the C-terminus, which is referred to as a C-terminal hydrophobic region (CHR); however, other enzymes have N-terminal membrane-bound helices or transmembrane regions.[64,65] CHR was identified using a SOSUI signal,[66] and this region was assumed to be the only membrane-bound site in FDH. However, an FDH variant deleting CHR (ΔCHR_FDH) was still localized to the membrane fraction, suggesting that subunit C contains additional membrane-bound sites.[67] The structure of FDH (including the CHR) was observed using cryo-electron microscopy (cryo-EM) analysis in 2022.[56] The CHR was confirmed to be in close proximity to the heme 1*c* region containing the UQ_{10}-binding site (Figure 1A). Therefore, the heme 1*c* region was assumed to be a membrane-bound site that could not be computationally estimated. Additionally, the improved performance of DET-type bioelectrocatalysis was hypothesized because of the surfactant-free solubilization of FDH.

In this study, a double variant (Δ1*c*ΔCHR_FDH) was constructed by deleting the heme 1*c* region (Pro27–Ile169) and CHR (Gly454–Trp476) in subunit C (Figure S1). Cryo-EM analysis was performed to structurally assess the advantages of Δ1*c*ΔCHR_FDH. The bioelectrochemical properties of Δ1*c*ΔCHR_FDH were then compared with those of rFDH and single variants (Δ1*c*_FDH and ΔCHR_FDH) using a multi-walled carbon nanotube (MWCNT) as an electrode. The suitability of CNTs as platforms for DET-type reactions of FDH have been previously reported.[43,50,54,56,68]

2. EXPERIMENTAL

2.1. Materials and reagents. MWCNTs (outer diameter: 10 ± 1 nm, inner diameter: 4.5 ± 0.5 nm, and length: 3–6 μm) were purchased from Sigma-Aldrich (USA). A protein ladder marker for sodium dodecyl sulfate-polyacrylamide gel electrophoresis (SDS-PAGE) was purchased from Nacalai Tesque (Japan). All other reagents were purchased from Wako Pure Chemical Industries (Japan). All aqueous solutions were prepared using distilled water. Bacterial strain and plasmids used in this study are summarized in Table S1. The *G. oxydans* NBRC12528 Δ*adhAB*Δ*aldFGH* strain[69] was used as an expression host. A plasmid for the expression of Δ1*c*ΔCHR_FDH was prepared by VectorBuilder, Japan.

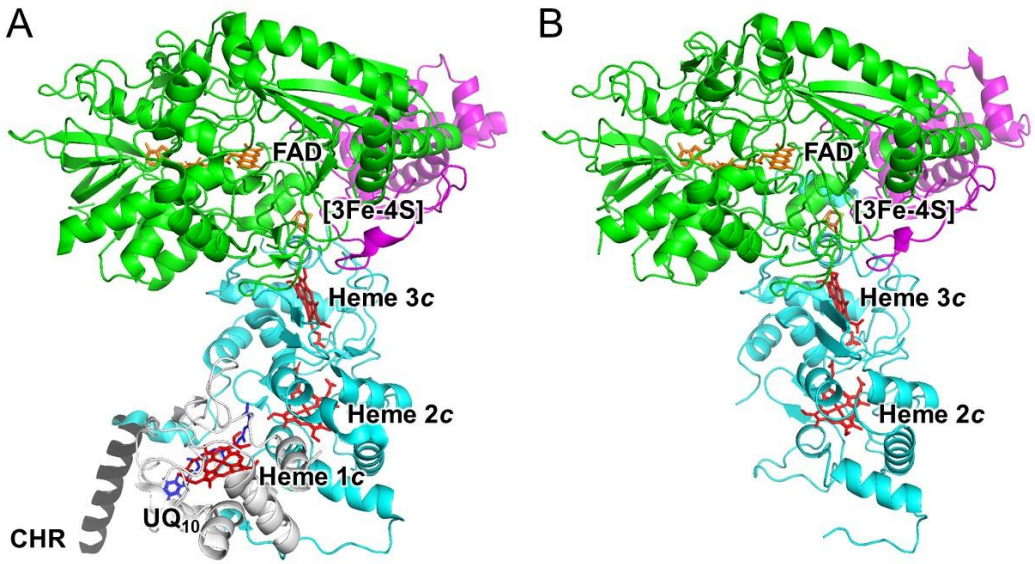

Figure 1. Structures of rFDH (A, PDB: 8JEJ and 7W2J) and Δ1*c*ΔCHR_FDH (B, PDB: 9JQA). Subunits L, S, and C are highlighted in green, magenta, and cyan, respectively. The heme 1*c* region and CHR are highlighted in white and black, respectively. Structure "A" is created by merging peptide chains of subunits L and S as well as all cofactors from the 8JEJ model and a peptide chain of subunit C from the 7W2J model. This was used to clarify the locations of UQ_{10} and CHR that were identified in monomeric and dimeric models, respectively.

2.2. Enzyme purification.

2.2.1. rFDH and Δ1*c*_FDH. rFDH and Δ1*c*_FDH were purified according to the procedure in the literature with several modifications.[57,70] All purification steps were performed at 4 °C. First, the collected cells were resuspended in 20 mM (M = mol dm^{-3}) phosphate buffer (pH 6.0), and disrupted twice at 100 MPa using a French Press (FA-080R, Thermo Fisher Scientific, USA). The removal of cell debris from the suspension was performed via centrifugation for 5 min at 12,000 × *g*. The supernatant was then centrifuged for 1 h at 100,000 × *g*. The enzyme was solubilized via the resuspension of the precipitated membrane fraction in 20 mM phosphate buffer (pH 6.0) containing 50 mM fructose, 1 mM 2-mercaptoethanol, 10% sucrose, and 1% Triton® X-100. The suspension was mixed for 8 h, then centrifuged for 1 h at 100,000 × *g*. The supernatant was added to a TOYOPEARL® DEAE-650M column (Tosoh Corporation, Japan), which was equilibrated with 20 mM phosphate buffer (pH 6.0) containing 5 mM fructose, 1 mM 2-mercaptoethanol, 10% sucrose, and 0.1% Triton® X-100. The column was washed using 5 column volumes of the same buffer. The flowthrough fraction was collected and applied to a CHT ceramic hydroxyapatite column (Bio-Rad, USA) equilibrated with the same buffer. The column was washed using 5 column volumes of 20 mM phosphate buffer (pH 6.0) containing 10% sucrose and 0.1% Triton® X-100 to remove fructose and 2-mercaptoethanol. rFDH and Δ1*c*_FDH were eluted using a linear concentration gradient (20–500 mM) of phosphate buffer (pH 6.0) containing 10% sucrose and 0.1% Triton® X-100. The purified enzyme was concentrated using ultrafiltration, then frozen in liquid nitrogen.

2.2.2. ΔCHR_FDH. ΔCHR_FDH was purified according to the procedure in the literature with several modifications.[66] The method described in Section 2.2.1. was followed until the flowthrough fraction was collected using a TOYOPEARL® DEAE-650M column. The flowthrough fraction was applied to a TOYOPEARL ® CM-650M column (Tosoh Corporation, Japan), which was equilibrated with 20 mM phosphate buffer (pH 6.0) containing 5 mM fructose, 1 mM 2-mercaptoethanol, 10% sucrose, and 0.1% Triton® X-100. The column was washed using 5 column volumes of 20 mM phosphate buffer (pH 6.0) containing 10% sucrose and 0.1% Triton® X-100 to remove fructose and 2-mercaptoethanol. ΔCHR_FDH was eluted using a linear concentration gradient (20–500 mM) of phosphate buffer (pH 6.0) containing 10% sucrose and 0.1% Triton® X-100. The purified enzyme was concentrated using ultrafiltration, then frozen in liquid nitrogen.

2.2.3. Δ1*c*ΔCHR_FDH. The collected cells were resuspended in 20 mM phosphate buffer (pH 6.0) containing 50 mM fructose, 1 mM 2-mercaptoethanol, and 10% sucrose, and disrupted twice at 100 MPa using a French Press. Cell debris was removed from the suspension via centrifugation for 5 min at 12,000 × *g*. The supernatant was centrifuged for 1 h at 100,000 × *g*. The membrane fraction had little activity for fructose oxidation, while the activity increased in the soluble fraction, owing to the deletion of the membrane-bound regions. Thereafter, the soluble fraction was applied to a TOYOPEARL® DEAE-650M column, which was equilibrated with 20 mM phosphate buffer (pH 6.0) containing 5 mM fructose, 1 mM 2-mercaptoethanol, and 10% sucrose. The column was washed using 5 column volumes of the same buffer. The flowthrough fraction was collected and applied to a CHT ceramic hydroxyapatite column equilibrated with the same buffer. The column was washed using 5 column volumes of the same buffer. The enzyme was eluted using a linear concentration gradient (20–500 mM) of phosphate buffer (pH 6.0) containing 5 mM fructose, 1 mM 2-mercaptoethanol, and 10% sucrose. After desalting via buffer exchange, the collected fraction was applied to a TOYOPEARL ® CM-650M column equilibrated with 20 mM phosphate buffer (pH 6.0) containing 5 mM fructose, 1 mM 2-mercaptoethanol, and 10% sucrose. The column was washed using 5 column volumes of 20 mM phosphate buffer (pH 6.0) containing 10% sucrose to remove fructose and 2-mercaptoethanol. Δ1*c*ΔCHR_FDH was eluted using a linear concentration gradient (20–500 mM) of phosphate buffer (pH 6.0) containing 10% sucrose. The purified enzyme was concentrated using ultrafiltration, then frozen in liquid nitrogen.

2.2.4. Enzyme assay. Figure S2 shows the SDS-PAGE results. Subunit C of each variant was successfully downsized. The protein concentrations were determined using a BCA protein assay kit (Thermo Fisher Scientific, USA), which employed bovine serum albumin as the standard. Spectrophotometric analysis of the fructose-oxidizing/ferricyanide-reducing activity of the enzymes was performed at 25 °C and pH 4.5 using a ferric-dupanol reagent.[71] One unit (U) was defined as the amount of enzyme that reacted with 1 μmol of fructose per minute.

2.3. Cryo-EM analysis of Δ1*c*ΔCHR_FDH.

2.3.1. Data collection. A 2.5-μL aliquot of the Δ1*c*ΔCHR_FDH solution (1 mg mL^{-1}) without sucrose was applied to a Quantifoil holey carbon support film grid (Cu R1.2/1.3), which was then frozen in liquid ethane using a FEI Vitrobot™ Mark IV (Thermo Fisher Scientific, USA) under conditions at 4 °C and 100 % humidity (L = dm^3). Blotting and drain time were set for 3 s and 2 s, respectively. Sample data were collected using a CRYO ARM 300 (JEOL, Japan) system equipped with a K3 direct electron detector camera (Gatan, USA), an Ω-type energy filter with a 20-eV slit width, and a cold field-emission electron gun operated at 300 kV. Images were recorded using Serial-EM[72] and holes were detected using YoneoLocr.[73] Movie frames were recorded using the K3 camera at a calibrated magnification of ×60,000, which was corresponding to a pixel size of 0.87 Å. The defocus range was set from −1.0 to −2.0 μm. These movie frames were recorded without gain normalization and with TIFF-LZW compression. The data collection was performed in counting mode, with a total dose of ~80 electrons $Å^{-2}$ and a total exposure of 3 s fractionated into 40 frames. Another grid was prepared with a 2.5-μL aliquot of the Δ1*c*ΔCHR_FDH solution (5 mg mL^{-1}) containing 0.9% *n*-octyl-β-D-glucoside (OG) in consideration of the preferred orientation challenge.[74] The data collection was conducted in the same procedure above. 7,091 and 12,975 movies were totally collected from the OG-uncontained and OG-contained grids, respectively.

2.3.2. Single particle analysis. Single particle analysis was performed using CryoSPARC ver. 4.2.0. After patch motion correction was performed to align all micrographs and estimate the contrast transfer function (CTF) parameters, particles representing proteins were automatically chosen by auto-picking, and the selected particles were extracted

into a box of 256 × 256 pixels. 7,016,675 particles were selected from 22,933,325 auto-picked particles using 2D classification. The initial 3D reference was obtained using ab-initio reconstruction. The first 3D classification (job name: heterogeneous refinement) into three classes with C1 symmetry showed a single clear class (3,932,443 particles). These processes were performed with binning by 4. After performing particle re-extraction into a box of 256 × 256 pixels from unbinning images, the second 3D classification into three classes with C1 symmetry showed a single clear class (1,987,357 particles). Subsequently, the selected particles were re-extracted into a box of 320 × 320 pixels after local motion correction. The third 3D classification into three classes with C1 symmetry showed a single clear class (1,703,212 particles). A final density map with a 2.15 Å resolution was obtained after Fourier shell correlation (FSC)-mask auto-tightening, subsequent homogenous refinement, and further CTF refinement. The whole process is summarized in Figure S3. The numerical data are listed in Table S2.

2.3.3. Molecular modeling. Atomic model building of Δ1*c*ΔCHR_FDH was performed using a Crystallographic Object-Oriented Toolkit (COOT). PHENIX was used for real-space refinement of the models based on the map of Δ1*c*ΔCHR_FDH obtained using cryo-EM. Cofactors were added based on previously described information.[56] The atomic models covered residues 2–542 in subunit L (541 residues), 177–444 in subunit C (268 residues), and 47–183 in subunit S (137 residues). The cryo-EM density map was deposited in the Electron Microscopy Data Bank with accession code EMD-61725. The atomic coordinate was deposited in the Protein Data Bank with the accession code 9JQA.

2.4. Electrode fabrication. Glassy carbon (GC) electrodes (diameter: 3 mm, BAS, Japan) were polished with 0.05-μm alumina slurry, sonicated, and washed using distilled water. MWCNTs were dispersed in *N*-methyl-2-pyrrolidone (NMP) at a final concentration of 1 mg mL^{-1} via sonication for 2 h. A 10-μL aliquot of the MWCNT dispersion was placed on the GC electrodes, and NMP was evaporated at 70 °C. This electrode was labelled CNT/GC. A 20-μL aliquot of the enzyme solution (1 mg mL^{-1}) was applied to the surface of the electrodes. The electrodes were left in a water-saturated atmosphere for 2 h at 4 °C. For rFDH, Δ1*c*_FDH, and ΔCHR_FDH, the enzymes were adsorbed on CNT/GCs in the presence of 0.1% Triton® X-100, while the Δ1*c*ΔCHR_FDH solution did not contain Triton® X-100. The electrodes were labelled rFDH/CNT/GC, Δ1*c*_FDH/CNT/GC, ΔCHR_FDH/CNT/GC, and Δ1*c*ΔCHR_FDH/CNT/GC, respectively.

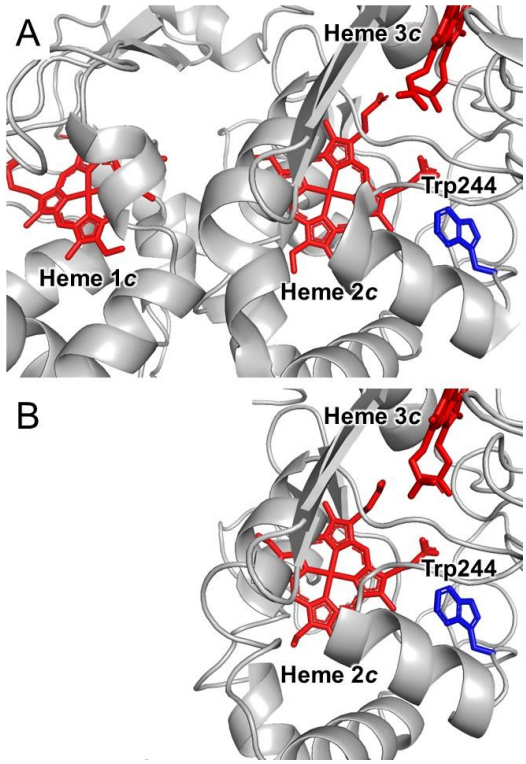

Figure 2. Local structures in proximity to the heme 2*c* of rFDH (A, PDB: 8JEJ) and Δ1*c*ΔCHR_FDH (B, PDB: 9JQA).

2.5. Electrochemical measurements. Electrochemical measurements were performed at 25 °C in McIlvaine buffer (pH 4.5) using a voltammetric analyzer (ALS650E, BAS, Japan) and a rotating disk electrode instrument (RRDE-3, BAS, Japan). Homemade Ag|AgCl|sat. KCl and platinum wire electrodes were used as reference and counter electrodes, respectively. All potentials in this study are shown against the reference electrode. Errors were identified using the Student's *t* distribution at a 90% confidence level.

3. RESULTS AND DISCUSSION

3.1. Structural properties of Δ1*c*ΔCHR_FDH. As mentioned in Section 2.2.3., Δ1*c*ΔCHR_FDH was purified without any surfactants. Therefore, FDH was proved to be bound to the membrane at both the heme 1*c* region and CHR. Figure 1B shows the 3D structure of Δ1*c*ΔCHR_FDH reconstructed based on the cryo-EM map at a resolution of 2.15 Å. The size of subunit C became smaller than that of rFDH as expected, whereas no conformational changes were observed in subunits L and S. The molecular mass of subunit C decreased by 35% (from 49 to 32 kDa) and 13% (from 130 to 113 kDa) for the heterotrimer owing to deletion. In addition, the single particle images obtained via cryo-EM analysis (Figure S3B) indicated that Δ1*c*ΔCHR_FDH is a monomer of the heterotrimer. A previous study showed that rFDH is a dimer of heterotrimers, and CHR anchors each other for stabilization in solution.[55] Therefore, the deletion of CHR contributed to the stabilization of Δ1*c*ΔCHR_FDH as a monomer.

Figure 2 shows the structures of rFDH and Δ1*c*ΔCHR_FDH in proximity of heme 2*c*. Heme 2*c* was exposed by the solvent owing to the deletion of the heme 1*c* region; however, the structure on the opposite side was well-conserved. Trp244 was particularly reported to be responsible for accelerating the long-range electron transfer from heme 2*c* to an electrode.[56] Therefore, the conserved position and angle of Trp244 indicate that the standard rate constant in the heterogeneous electron transfer ($k°$) of Δ1*c*ΔCHR_FDH is as high as that of rFDH. Because the intramolecular electron transfer pathway from FAD to heme 2*c* was also conserved in Δ1*c*ΔCHR_FDH, the catalytic constant in DET-type bioelectrocatalysis (k_c) was likely equal between rFDH and Δ1*c*ΔCHR_FDH. Assuming that unintended conformational changes do not occur in single variants (Δ1*c*_FDH and ΔCHR_FDH), no changes to the $k°$ and k_c values of Δ1*c*_FDH and ΔCHR_FDH should be observed. These suggestions were investigated in the following sections.

The ferricyanide-reducing activities in solution of rFDH, Δ1*c*_FDH, ΔCHR_FDH, and Δ1*c*ΔCHR_FDH were 1170 ± 50, 740 ± 50, 780 ± 90, and 780 ± 90 U mg^{-1}, respectively. A reduction in the activity for variants is likely owing to the deletion of the heme 1*c* region and/or CHR. This result indicates that the catalytic cycle of FDH in solution is somewhat kinetically controlled by a ferricyanide-reducing process at hemes 1*c* or 2*c*.

3.2. Bioelectrochemical characterization of Δ1*c*ΔCHR_FDH. Cyclic voltammograms (CVs) recorded at enzyme-modified CNT/GCs are shown in Figure 3. All electrodes exhibited sigmoidal catalytic waves derived from fructose oxidation. The catalytic current densities of rFDH, Δ1*c*_FDH, ΔCHR_FDH, and Δ1*c*ΔCHR_FDH at 0.5 V were 0.8 ± 0.1, 2.4 ± 0.3, 0.32 ± 0.06, and 11 ± 1 mA cm^{-2}, respectively. The rates of the change in catalytic current relative to rFDH were 3.0 ± 0.5, 0.40 ± 0.09, and 14 ± 3 for Δ1*c*_FDH, ΔCHR_FDH, and Δ1*c*ΔCHR_FDH, respectively. Δ1*c*ΔCHR_FDH exhibited improved DET-type bioelectrocatalysis. This result suggests that downsizing the enzyme and removing surfactants increased the surface concentration of the enzyme effective for DET ($\Gamma_{E,eff}$). The effect of downsizing was also confirmed at the Δ1*c*_FDH/CNT/GC; however, the rate of increase in the catalytic current (3.0 ± 0.5) was much higher than the value simply estimated from the actual downsizing rate (13%). This contradiction suggests that the enzyme orientation at the electrode surface can be improved by deleting the heme 1*c* region. However, distinct non-catalytic redox signals of the enzyme were not observed in the CVs of all variants in the absence of fructose (Figure S4), compared with CVs of the enzyme-unmodified CNT/GC (Figure S5). Therefore, $\Gamma_{E,eff}$ cannot be electrochemically estimated.

Δ1*c*ΔCHR_FDH/CNT/GC was prepared with the Δ1*c*ΔCHR_FDH solution containing 0.1% Triton® X-100 to estimate the level of interference by surfactants. The current density of the electrode (1.5 ± 0.3 mA cm^{-2} at 0.5 V) was approximately 90% lower than that prepared without Triton® X-100 (Figure 4). This result indicates that the surface of the electrode can adsorb Triton® X-100; therefore, Triton® X-100 and the enzyme compete for access to the surface of the electrode. Furthermore, although the sizes of Δ1*c*ΔCHR_FDH and Δ1*c*_FDH were similar, the current density of the Δ1*c*ΔCHR_FDH/CNT/GC prepared with Triton® X-100 was lower than that of Δ1*c*_FDH/CNT/GC. Therefore, Δ1*c*ΔCHR_FDH likely exhibited weaker hydrophobic interactions with MWCNTs than those of Δ1*c*_FDH and Triton® X-100 because of the deletion of CHR. This finding was consistent with that of the difference in catalytic current density between ΔCHR_FDH and rFDH.

3.3. Kinetic analysis of voltammograms. To quantitatively evaluate the kinetic and thermodynamic parameters of FDH variants, the voltammograms were analyzed using the DET-type bioelectrocatalysis model as follows.[75]

$$j = \frac{n_S F k_c \Gamma_{E,eff}}{1 + \frac{k_c}{k_f} + \frac{k_b}{k_f}} \quad (1)$$

In Equation (1), n_S is the electron number of substrate oxidation (2 in this instance), and F is the Faraday constant. k_f and k_b are the heterogeneous electron transfer rate constants for oxidation and reduction, respectively, as described by the following Butler–Volmer equation.

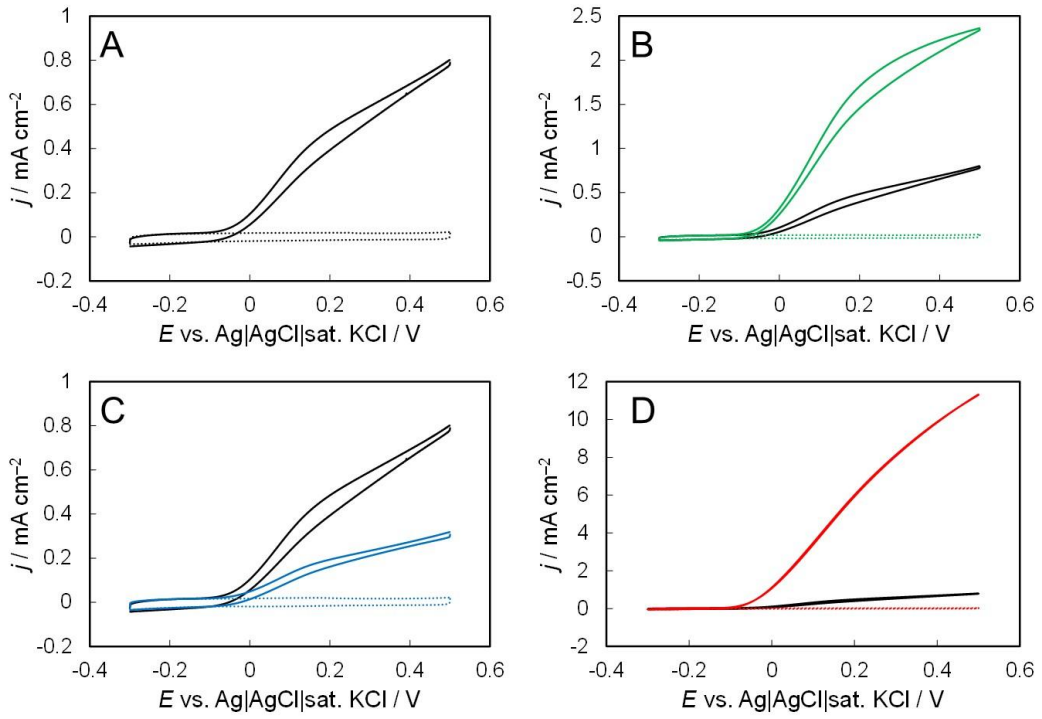

Figure 3. CVs representing DET-type fructose oxidation at (A) rFDH/CNT/GC, (B) Δ1*c*_FDH/CNT/GC, (C) ΔCHR_FDH/CNT/GC, and (D) Δ1*c*ΔCHR_FDH/CNT/GC. Measurements were performed in McIlvaine buffer (pH 4.5) containing 100 mM D-fructose under Ar-saturated conditions at 25 °C, a scan rate (v) of 10 mV s^{-1}, and a rotation speed (ω) of 4000 rpm (solid lines). Dotted lines indicate CVs in the absence of D-fructose. Black lines in B, C, and D indicate CVs at rFDH/CNT/GC.

$$k_f = k^\circ \exp\left\{\frac{(1-\alpha)n'_E F}{RT}(E - E^{\circ\prime}_E)\right\} \quad (2)$$

$$k_b = k^\circ \exp\left\{-\frac{\alpha n'_E F}{RT}(E - E^{\circ\prime}_E)\right\} \quad (3)$$

α is the transfer coefficient (generally a value of 0.5), n'_E is the electron number of heterogeneous electron transfer (generally a value of 1), $E^{\circ\prime}_E$ is the formal potential of the electrode-active cofactor of the enzyme (heme 2*c* in this instance), R is the gas constant, and T is the absolute temperature. To incorporate the enzyme orientation in the model, four k° values were distributed: k_1 (k°_{max}; the maximum k°), k_2 ($k^\circ_{max}/10$), k_3 ($k^\circ_{max}/10^2$), and k_4 ($k^\circ_{max}/10^3$). The proportion of k° was set to p_1, p_2, p_3, and p_4 ($1 - p_1 - p_2 - p_3$), which corresponded to k_1, k_2, k_3, and k_4, respectively. Therefore, Equation (1) can be rewritten as follows.

$$j = n_S F k_c \Gamma_{E,eff} \sum_{n=1}^{4} p_n \left\{1 + \left(\frac{k^\circ_{max}}{k_c}\frac{\eta^{1-\alpha}}{10^{n-1}}\right)^{-1} + \eta^{-1}\right\}^{-1} \quad (4)$$

$$\eta = \exp\left\{\frac{n'_E F}{RT}(E - E^{\circ\prime}_E)\right\} \quad (5)$$

Using $k_c\Gamma_{E,eff}$, k°_{max}/k_c, $E^{\circ\prime}_E$, p_1, p_2, and p_3 as adjustable parameters, Equation (4) was fitted to voltammograms based on the non-linear regression analysis calculated by Gnuplot®. Refined parameters are summarized in Table 1. Refined curves are shown in Figure 5.

Based on the aforementioned structural information, the value of k_c was likely constant in the presence or absence of the heme 1*c* region and/or CHR. Therefore, the $\Gamma_{E,eff}$ and k°_{max} values can be compared using the $k_c\Gamma_{E,eff}$ and k°_{max}/k_c values, respectively. Discussion on $\Gamma_{E,eff}$ is identical to the description in Section 3.2., that is, effects of downsizing of the enzyme and interference of surfactants were suggested for the variants. The k°_{max} values of rFDH and its variants were similar. This result is consistent with the structural information that the interfacial electron transfer pathway from heme 2*c* to the electrode is conserved between rFDH and Δ1*c*ΔCHR_FDH.

The $E^{\circ\prime}_E$ values of rFDH and its variants were similar when the condition for electrode fabrication was standardized to include Triton® X-100 in the enzyme solution. This indicates that the formal potential of heme 2*c* was not affected by the deletion of the heme 1*c* region and/or CHR. In contrast, a negative shift in $E^{\circ\prime}_E$ by approximately 15 mV was observed for Δ1*c*ΔCHR_FDH in the absence of Triton® X-100. Because the heme 2*c* of Δ1*c*ΔCHR_FDH was exposed by the solvent (Figure 2), the presence of Triton® X-100 may have altered the formal potential of heme 2*c*. A similar interaction between hemin and surfactants were reported using microperoxidase 11.[76]

Differences in the enzyme orientation of rFDH and its variants were clarified. The p_1 and p_2 values of Δ1*c*_FDH were

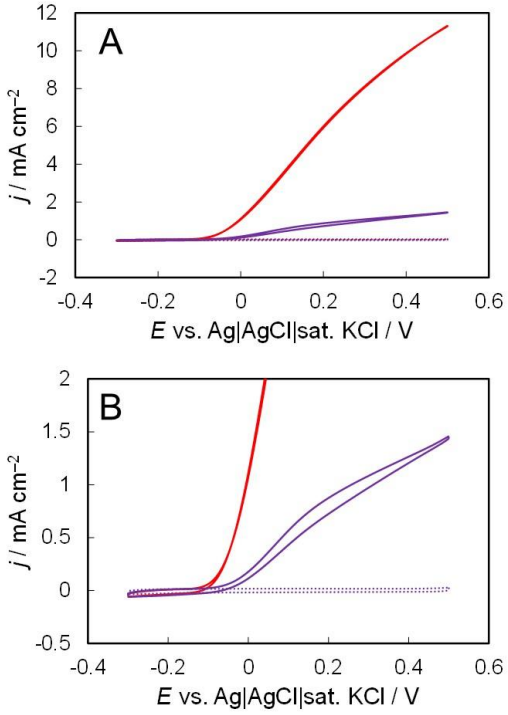

Figure 4. (A) CVs recorded at Δ1*c*ΔCHR_FDH/CNT/GC prepared with Triton® X-100. Measurements were performed in McIlvaine buffer (pH 4.5) containing 100 mM D-fructose under Ar-saturated conditions at 25 °C, ν = 10 mV s^{-1}, and ω = 4000 rpm (solid line). A Dotted line indicates a CV in the absence of D-fructose. A red line indicates a CV at Δ1*c*ΔCHR_FDH/CNT/GC prepared without Triton® X-100.
(B) Enlarged view of A.

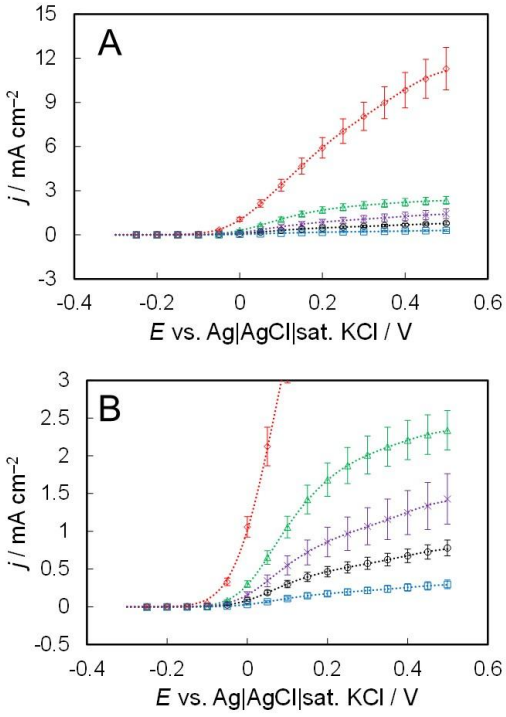

Figure 5. (A) Background-subtracted voltammograms representing the DET-type fructose oxidation at rFDH/CNT/GC (black circles), Δ1*c*_FDH/CNT/GC (green triangles), ΔCHR_FDH/CNT/GC (blue squares), Δ1*c*ΔCHR_FDH/CNT/GC prepared without Triton® X-100 (red diamonds), and Δ1*c*ΔCHR_FDH/CNT/GC prepared with Triton® X-100 (purple crosses). Dotted lines indicate refined curves obtained by regression analysis.
(B) Enlarged view of A.

Table 1. Refined parameters for rFDH and its variants.

	$k_c\Gamma_{E,eff}$ / nmol cm^{-2}	$k^{\circ}{}_{max}/k_c$	$E^{\circ\prime}{}_E$ / mV	p_1 / %	p_2 / %	p_3 / %	p_4 / %
rFDH	4.1 ± 0.5	0.32 ± 0.04	−2 ± 5	50 ± 2	15 ± 1	10 ± 1	24 ± 1
Δ1*c*_FDH	12 ± 1	0.35 ± 0.01	2 ± 1	57 ± 2	25 ± 1	7 ± 1	10 ± 1
ΔCHR_FDH	1.6 ± 0.3	0.28 ± 0.02	−5 ± 4	49 ± 2	15 ± 2	10 ± 1	25 ± 3
Δ1*c*ΔCHR_FDH (prepared without Triton® X-100)	60 ± 8	0.28 ± 0.02	−18 ± 3	31 ± 3	28 ± 2	16 ± 1	24 ± 2
Δ1*c*ΔCHR_FDH (prepared with Triton® X-100)	8 ± 2	0.34 ± 0.03	−3 ± 2	47 ± 2	20 ± 6	10 ± 1	23 ± 2

higher than those of rFDH. Therefore, Δ1*c*_FDH exhibited improved enzymatic orientation compared with that of rFDH. In contrast, the p_1 value of Δ1*c*ΔCHR_FDH was lower than that of rFDH, Δ1*c*_FDH, and ΔCHR_FDH. However, the p_1 value increases in the presence of Triton® X-100, suggesting that the incorporation of surfactants control the orientation of FDH for DET. These results corroborate the findings of a previous study, which showed that the DET activity of FDH at thiol-modified gold electrodes depended on the hydrophobicity and hydrophilicity of the surface of the electrode.[38]

Compared with rFDH and the other variants, Δ1*c*ΔCHR_FDH exhibited the highest performance for DET-type fructose oxidation based on the quantitative analysis of kinetic and thermodynamic parameters. The downsized surfactant-free variant exhibited a 14-fold higher catalytic current density than that of rFDH. A 10-mV reduction in the overpotential was also attained. However, the removal of surfactants marginally reduced the precision of the orientation of the enzyme. DET-type bioelectrocatalysis can be improved by implementing various techniques for electrode functionalization and protein engineering.

4. CONCLUSIONS

The DET-type bioelectrocatalysis of FDH was improved by using a variant truncating the heme 1*c* region and CHR. The double variant, Δ1*c*ΔCHR_FDH, was expressed in the soluble fraction owing to the deletion of membrane-bound regions of FDH. Cryo-EM analysis revealed that Δ1*c*ΔCHR_FDH was downsized without the occurrence of conformational changes that can interfere with its catalytic activity. An increase in the $\Gamma_{E,eff}$ value of Δ1*c*ΔCHR_FDH at the MWCNT electrode was attributed to the effects of the downsizing of the enzyme and removal of surfactants. As a result, Δ1*c*ΔCHR_FDH exhibited a 14-fold higher catalytic current density than that of rFDH. Kinetic analysis of voltammograms showed that the addition of surfactants resulted in a marginal change in $E^{\circ\prime}{}_E$ and improved the orientation of the enzyme. Similar approaches can improve other membrane-bound DET-type enzymes. This study improves the understanding of the structural mechanism of membrane-bound proteins and represents a step forward in the development of DET-based bioelectrochemical system.

ASSOCIATED CONTENT

Supporting Information

SDS-PAGE of the enzymes, bacterial strains, plasmids, and additional structural and electrochemical data are described in the Supporting Information.
This material is available free of charge via the Internet at http://pubs.acs.org.XXXXXXX.

AUTHOR INFORMATION

Corresponding Author

Keisei Sowa – Division of Applied Life Sciences, Graduate School of Agriculture, Kyoto University, Sakyo, Kyoto 606-8502, Japan, orcid.org/0000-0001-9767-4922; E-mail: sowa.keisei.2u@kyoto-u.ac.jp

Authors

Taiki Adachi – Division of Applied Life Sciences, Graduate School of Agriculture, Kyoto University, Sakyo, Kyoto 606-8502, Japan, orcid.org/0000-0002-3863-993X
Konatsu Ichikawa – Division of Applied Life Sciences, Graduate School of Agriculture, Kyoto University, Sakyo, Kyoto 606-8502, Japan, orcid.org/0009-0004-5386-378X
Tomoko Miyata – Graduate School of Frontier Biosciences, Osaka University, Suita, Osaka 565-0871, Japan, orcid.org/0000-0002-5543-7459
Fumiaki Makino – Graduate School of Frontier Biosciences, Osaka University, Suita, Osaka 565-0871, Japan; JEOL Ltd., Akishima, Tokyo 196-8558, Japan, orcid.org/0000-0001-9512-7087
Hideaki Tanaka – TechnoPro R&D Company, Kobe, Hyogo 650-0047, Japan, orcid.org/0000-0003-2035-954X
Keiichi Namba – Graduate School of Frontier Biosciences, Osaka University, Suita, Osaka 565-0871, Japan; RIKEN Center for Biosystems Dynamics Research, Suita, Osaka 565-0874, Japan; RIKEN SPring-8 Center, Sayo, Hyogo 679-5198, Japan, orcid.org/0000-0003-2911-5875

Funding Sources

Platform Project for Supporting Drug Discovery and Life Science Research (Basis for Supporting Innovative Drug Discovery and Life Science Research (BINDS)) from AMED (Grant Number JP23ama121003). JSPS KAKENHI (Grant Numbers JP23K19281 and JP22K14831). FY 2022 Kusunoki 125 of

Kyoto University 125th Anniversary Fund. GteX Program of Japan (Grant Number JPMJGX23B4).

Notes

The authors declare no competing financial interest.

ACKNOWLEDGMENTS

This research was supported by the Platform Project for Supporting Drug Discovery and Life Science Research (Basis for Supporting Innovative Drug Discovery and Life Science Research (BINDS)) from AMED under grant number JP23ama121003 to K.N., JSPS KAKENHI under grant numbers JP22K14831 to K.S. and JP23K19281 to T.A., and FY 2022 Kusunoki 125 of Kyoto University 125th Anniversary Fund to K.S. This study was supported by the GteX Program of Japan Grant Number JPMJGX23B4 to K.S. We express our gratitude to Hirou Kaku, Koryu Ou, and Yasuyuki Hamano for their financial support. We would also like to thank Editage (www.editage.com) for the English-language editing.

ABBREVIATIONS

CHR, C-terminal hydrophobic region; Cryo-EM, cryo-electron microscopy; DET, direct electron transfer; FAD, flavin adenine dinucleotide; FDH, fructose dehydrogenase; GC, glassy carbon; MWCNT, multi-walled carbon nanotube; OG, *n*-octyl-β-D-glucoside; SDS-PAGE, sodium dodecyl sulfate-polyacrylamide gel electrophoresis; UQ_{10}, ubiquinone-10.

REFERENCES

(1) Léger, C.; Bertrand, P. Direct Electrochemistry of Redox Enzymes as Tool for Mechanistic Studies. *Chem. Rev.* **2008**, *108* (7), 2379–2438. https://doi.org/10.1021/cr0680742

(2) Fourmond, V.; Léger, C. Modelling the Voltammetry of Adsorbed Enzymes and Molecular Catalysts. *Curr. Opin. Electrochem.* **2017**, *1* (1), 110–120. https://doi.org/10.1016/j.coelec.2016.11.002

(3) Milton, R. D.; Minteer, S. D. Direct Enzymatic Bioelectrocatalysis: Differentiating between Myth and Reality. *J. R. Soc. Interface* **2017**, *14* (131), 20170253. https://doi.org/10.1098/rsif.2017.0253

(4) Sensi, M.; del Barrio, M.; Baffert, C.; Fourmond, V.; Léger, C. New Perspectives in Hydrogenase Direct Electrochemistry. *Curr. Opin. Electrochem.* **2017**, *5* (1), 135–145. https://doi.org/10.1016/j.coelec.2017.08.005

(5) Armstrong, F. A. Some Fundamental Insights into Biological Redox Catalysis from the Electrochemical Characteristics of Enzymes Attached Directly to Electrodes. *Electrochim. Acta* **2021**, *390*, 138836. https://doi.org/10.1016/j.electacta.2021.138836

(6) Lojou, E.; Xiao, X. Enzymatic Bioelectrocatalysis. *Catalysts* **2021**, *11* (11), 1373. https://doi.org/10.3390/catal11111373

(7) Willner, I.; Katz, E.; Willner, B. Electrical Contact of Redox Enzyme Layers Associated with Electrodes; Routes to Amperometric Biosensors. *Electroanalysis* **1997**, *9* (13), 965–977. https://doi.org/10.1002/elan.1140091302

(8) Thévenot, D. R.; Tóth, K.; Durst, R. A.; Wilson, G. Electrochemical Biosensors: Recommended Definitions and Classification. *Pure Appl. Chem.* **1999**, *71* (1–2), 2333–2348. https://doi.org/10.1016/s0956-5663(01)00115-4

(9) Scheller, F. W.; Wollenberger, U.; Warsinke, A.; Lisdat, F. Research and Development in Biosensors. *Curr. Opin. Biotechnol.* **2001**, *12* (1), 35–40. https://doi.org/10.1016/S0958-1669(00)00169-5

(10) Bollella, P.; Gorton, L. Enzyme Based Amperometric Biosensors. *Curr. Opin. Electrochem.* **2018**, *10*, 157–173. https://doi.org/10.1016/j.coelec.2018.06.003

(11) Bollella, P.; Gorton, L.; Antiochia, R. Direct Electron Transfer of Dehydrogenases for Development of 3rd Generation Biosensors and Enzymatic Fuel Cells. *Sensors* **2018**, *18* (5), 1319. https://doi.org/10.3390/s18051319

(12) Kucherenko, I. S.; Soldatkin, O. O.; Kucherenko, D. Y.; Soldatkina, O. V.; Dzyadevych, S. V. Advances in Nanomaterial Application in Enzyme-Based Electrochemical Biosensors. *Nanoscale Adv.* **2019**, *1* (12), 4560–4577. https://doi.org/10.1039/C9NA00491B

(13) Ngyen, H. H.; Lee, S. H.; Lee, U. J.; Fermin, C. D.; Kim, M. Immobilized Enzymes in Biosensor Applications. *Materials* **2019**, *12* (1), 121. https://doi.org/10.3390%2Fma12010121

(14) Pinyou, P.; Blay, V.; Muresan, L. M.; Noguer, T. Enzyme-Modified Electrodes for Biosensors and Biofuel Cells. *Mater. Horiz.* **2019**, *6* (7), 1336–1358. https://doi.org/10.1039/C9MH00013E

(15) Bollella, P.; Katz, E. Enzyme-Based Biosensors: Tackling Electron Transfer Issues. *Sensors* **2020**, *20* (12), 3517. https://doi.org/10.3390%2Fs20123517

(16) Franco, J. H.; Minteer, S. D.; de Andrade, A. R. Ethanol Biofuel Cells: Hybrid Catalytic Cascades as a Tool for Biosensor Devices. *Biosensors* **2021**, *11* (2), 41. https://doi.org/10.3390/bios11020041

(17) Barton, S. C.; Gallaway, J.; Atanassov, P. Enzymatic Biofuel Cells for Implantable and Microscale Devices. *Chem. Rev.* **2004**, *104* (10), 4867–4886. https://doi.org/10.1021/cr020719k

(18) Cracknell, J. A.; Vincent, K. A.; Armstrong, F. A. Enzymes as Working or Inspirational Electrocatalysts for Fuel Cells and Electrolysis. *Chem. Rev.* **2008**, *108* (7), 2439–2461. https://doi.org/10.1021/cr0680639

(19) Meredith, M. T.; Minteer, S. D. Biofuel Cells; Enhanced Enzymatic Bioelectrocatalysis. *Annu. Rev. Anal. Chem.* **2012**, *5*, 157–179. https://doi.org/10.1146/annurev-anchem-062011-143049

(20) de Poulpiquet, A.; Ranava, D.; Monsalve, K.; Giudici-Orticoni, M.-T.; Lojou, E. Biohydrogen for a New Generation of H_2/O_2 Biofuel Cells: A Sustainable Energy Perspective. *ChemElectroChem* **2014**, *1* (11), 1724–1750. https://doi.org/10.1002/celc.201402249

(21) Mano, N.; de Poulpiquet, A. O_2 Reduction in Enzymatic Biofuel Cells. *Chem. Rev.* **2018**, *118* (5), 2392–2468. https://doi.org/10.1021/acs.chemrev.7b00220

(22) Xiao, X.; Xia, H.-Q.; Wu, R.; Bai, L.; Yan, L.; Magner, E.; Cosnier, S.; Lojou, E.; Zhu, Z.; Liu, A. Tackling the Challenges of Enzymatic (Bio)Fuel Cells. *Chem. Rev.* **2019**, *119* (16), 9509–9558. https://doi.org/10.1021/acs.chemrev.9b00115

(23) Shleev, S.; González-Arribas, E.; Falk, M. Biosupercapacitors. *Curr. Opin. Electrochem.* **2017**, *5* (1), 226–233. https://doi.org/10.1016/j.coelec.2017.09.023

(24) Krieg, T.; Sydow, A.; Schröder, U.; Schrader, J.; Holtmann, D. Reactor Concepts for Bioelectrochemical Syntheses and Energy Conversion. *Trends Biotechnol.* **2014**, *32* (12), 645–655. https://doi.org/10.1016/j.tibtech.2014.10.004

(25) Milton, R. D.; Minteer, S. D. Enzymatic Bioelectrosynthetic Ammonia Production: Recent Electrochemistry of Nitrogenase, Nitrate Reductase, and Nitrite Reductase. *ChemPlusChem* **2017**, *82* (4), 513–521. https://doi.org/10.1002/cplu.201600442

(26) Adachi, T.; Kitazumi, Y.; Shirai, O.; Kano, K. Recent Progress in Applications of Enzymatic Bioelectrocatalysis. *Catalysts* **2020**, *10* (12), 1413. https://doi.org/10.3390/catal10121413

(27) Lee, Y. S.; Lim, K.; Minteer, S. D. Cascaded Biocatalysis and Bioelectrocatalysis: Overview and Recent Advances. *Annu. Rev. Phys. Chem.* 2021, 72, 467–488. https://doi.org/10.1146/annurev-physchem-090519-050109

(28) Siritanaratkul, B.; Megarity, C. F. Electrochemically-Driven Enzyme Cascades: Recent Developments in Design, Control, and Modelling. *Curr. Opin. Electrochem.* **2024**, *47*, 101565. https://doi.org/10.1016/j.coelec.2024.101565

(29) Bollella, P.; Ludwig, R.; Gorton, L. Cellobiose Dehydrogenase: Insights on the Nanostructuration of Electrodes for Improved Development of Biosensors and Biofuel Cells. *Appl. Mater. Today* **2017**, *9*, 319–332. https://doi.org/10.1016/j.apmt.2017.08.009
(30) Mazurenko, I.; de Poulpiquet, A.; Lojou, E. Recent Developments in High Surface Area Bioelectrodes for Enzymatic Fuel Cells. *Curr. Opin. Electrochem.* **2017**, *5* (1), 74–84. https://doi.org/10.1016/j.coelec.2017.07.001
(31) Yates, N. D. J.; Fascione, M. A.; Parkin, A. Methodologies for "Wiring" Redox Proteins/Enzymes to Electrode Surfaces. *Chem. Eur. J.* **2018**, *24* (47), 12164–12182. https://doi.org/10.1002/chem.201800750
(32) Adachi, T.; Kitazumi, Y.; Shirai, O.; Kano, K. Direct Electron Transfer-Type Bioelectrocatalysis of Redox Enzymes at Nanostructured Electrodes. *Catalysts* **2020**, *10* (2), 236. https://doi.org/10.3390/catal10020236
(33) Bollella, P.; Katz, E. Bioelectrocatalysis at Carbon Nanotubes. *Methods Enzymol.* **2020**, *630*, 215–247. https://doi.org/10.1016/bs.mie.2019.10.012
(34) Mazurenko, I.; Hitaishi, V. P.; Lojou, E. Recent Advances in Surface Chemistry of Electrodes to Promote Direct Enzymatic Bioelectrocatalysis. *Curr. Opin. Electrochem.* **2020**, *19*, 113–121. https://doi.org/10.1016/j.coelec.2019.11.004
(35) Sugimoto, Y.; Takeuchi, R.; Kitazumi, Y.; Shirai, O.; Kano, K. Significance of Mesoporous Electrodes for Noncatalytic Faradaic Process of Randomly Oriented Redox Proteins. *J. Phys. Chem. C* **2016**, *120* (46), 26270–26277. https://doi.org/10.1021/acs.jpcc.6b07413
(36) Sugimoto, Y.; Kitazumi, Y.; Shirai, O.; Kano, K. Effects of Mesoporous Structures on Direct Electron Transfer-Type Bioelectrocatalysis: Facts and Simulation on a Three-Dimensional Model of Random Orientation of Enzymes. *Electrochemistry* **2017**, *85* (2), 82–87. https://doi.org/10.5796/electrochemistry.85.82
(37) Kitazumi, Y.; Shirai, O.; Yamamoto, M.; Kano, K. Numerical Simulation of Diffuse Double Layer around Microporous Electrodes Based on the Poisson–Boltzmann Equation. *Electrochim. Acta* **2013**, *112*, 171–175. https://doi.org/10.1016/j.electacta.2013.08.117
(38) Kawai, S.; Yakushi, T.; Matsushita, K.; Kitazumi, Y.; Shirai, O.; Kano, K. Role of a Non-Ionic Surfactant in Direct Electron Transfer-Type Bioelectrocatalysis by Fructose Dehydrogenase. *Electrochim. Acta* **2015**, *152*, 19–24. https://doi.org/10.1016/j.electacta.2014.11.113
(39) Adachi, T.; Kaida, Y.; Kitazumi, Y.; Shirai, O.; Kano, K. Bioelectrocatalytic Performance of D-Fructose Dehydrogenase. *Bioelectrochemistry* **2019**, *129*, 1–9. https://doi.org/10.1016/j.bioelechem.2019.04.024
(40) Ikeda, T.; Matsushita, F.; Senda, M. Amperometric Fructose Sensor Based on Direct Bioelectrocatalysis. *Biosens. Bioelectron.* **1991**, *6* (4), 299–304. https://doi.org/10.1016/0956-5663(91)85015-O
(41) Parellada, J.; Domínguez, E.; Fernández, V. M. Amperometric Flow Injection Determination of Fructose in Honey with a Carbon Paste Sensor Based on Fructose Dehydrogenase. *Anal. Chim. Acta* **1996**, *330* (1), 71–77. https://doi.org/10.1016/0003-2670(96)87686-0
(42) Yabuki, S.; Mizutani, F. D-Fructose Sensing Electrode Based on Electron Transfer of D-Fructose Dehydrogenase at Colloidal Gold-Enzyme-Modified Electrode. *Electroanalysis* **1997**, *9* (1), 23–25. https://doi.org/10.1002/elan.1140090107
(43) Tominaga, M.; Nomura, S.; Taniguchi, I. D-Fructose Detection Based on the Direct Heterogeneous Electron Transfer Reaction of Fructose Dehydrogenase Adsorbed onto Multi-Walled Carbon Nanotubes Synthesized on Platinum Electrode. *Biosens. Bioelectron.* **2009**, *24* (5), 1184–1188. https://doi.org/10.1016/j.bios.2008.07.002
(44) Tsujimura, S.; Nishina, A.; Kamitaka, Y.; Kano, K. Coulometric D-Fructose Biosensor Based on Direct Electron Transfer Using D-Fructose Dehydrogenase. *Anal. Chem.* **2009**, *81* (22), 9383–9387. https://doi.org/10.1021/ac901771t
(45) Šakinytė, I.; Barkauskas, J.; Gaidukevič, J.; Razumienė, J. Thermally Reduced Graphene Oxide: The Study and Use for Reagentless Amperometric D-Fructose Biosensors. *Talanta* **2015**, *144*, 1096–1103. https://doi.org/10.1016/j.talanta.2015.07.072
(46) Siepenkoetter, T.; Salaj-Kosla, U.; Magner, E. The Immobilization of Fructose Dehydrogenase on Nanoporous Gold Electrodes for the Detection of Fructose. *ChemElectroChem* **2017**, *4* (4), 905–912. https://doi.org/10.1002/celc.201600842
(47) Bollella, P.; Hibino Y.; Kano, K.; Gorton L.; Antiochia R. Highly Sensitive Membraneless Fructose Biosensor Based on Fructose Dehydrogenase Immobilized onto Aryl Thiol Modified Highly Porous Gold Electrode: Characterization and Application in Food Samples. *Anal. Chem.* **2018**, *90* (20), 12131–12136. https://doi.org/10.1021/acs.analchem.8b03093
(48) Okawa, Y.; Shimada, T.; Shiba, F. Formation of Gold-Silver Hollow Nanostructure via Silver Halide Photographic Processes and Application to Direct Electron Transfer Biosensor Using Fructose Dehydrogenase. *J. Electroanal. Chem.* **2018**, *828*, 144–149. https://doi.org/10.1016/j.jelechem.2018.09.044
(49) Suzuki, Y.; Kano, K.; Shirai, O.; Kitazumi, Y. Diffusion-Limited Electrochemical D-Fructose Sensor Based on Direct Electron Transfer-Type Bioelectrocatalysis by a Variant of D-Fructose Dehydrogenase at a Porous Gold Microelectrode. *J. Electroanal. Chem.* **2020**, *877*, 114651. https://doi.org/10.1016/j.jelechem.2020.114651
(50) Bollella, P.; Boeva, Z.; Latonen, R.-M.; Kano, K.; Gorton, L.; Bobacka, J. Highly Sensitive and Stable Fructose Self-Powered Biosensor Based on a Self-Charging Biosupercapacitor. *Biosens. Bioelectron.* **2021**, *176*, 112909. https://doi.org/10.1016/j.bios.2020.112909
(51) Silveri, F.; Paolini, D.; Pelle, F. D.; Bollella, P.; Scroccarello, A.; Suzuki, Y.; Fukawa, E.; Sowa, K.; Franco, C. D.; Torsi, L.; Compagnone, D. Lab-Made Flexible Third-Generation Fructose Biosensors Based on 0D-Nanostructured Transducers. *Biosens. Bioelectron.* **2023**, *237*, 115450. https://doi.org/10.1016/j.bios.2023.115450
(52) Silveri, F.; Pelle, F. D.; Scroccarello, A.; Bollella, P.; Ferraro, G.; Fukawa, E.; Suzuki, Y.; Sowa, K.; Torsi, L.; Compagnone, D. Exploiting CO_2 Laser to Boost Graphite Inks Electron Transfer for Fructose Biosensing in Biological Fluids. *Biosens. Bioelectron.* **2024**, *263*, 116620. https://doi.org/10.1016/j.bios.2024.116620
(53) Kamitaka, Y.; Tsujimura, S.; Setoyama, N.; Kajino, T.; Kano, K. Fructose/Dioxygen Biofuel Cell Based on Direct Electron Transfer-Type Bioelectrocatalysis. *Phys. Chem. Chem. Phys.* **2007**, *9* (15), 1793–1801. https://doi.org/10.1039/B617650J
(54) Wu, X.; Zhao, F.; Varcoe, J. R.; Thumser, A. E.; Avignone-Rossa, C.; Slade, R. C. T. A One-Compartment Fructose/Air Biological Fuel Cell Based on Direct Electron Transfer. *Biosens. Bioelectron.* **2009**, *25* (2), 326–331. https://doi.org/10.1016/j.bios.2009.07.011
(55) So, K.; Kawai, S.; Hamano, Y.; Kitazumi, Y.; Shirai, O.; Hibi, M.; Ogawa, J.; Kano, K. Improvement of a Direct Electron Transfer-Type Fructose/Dioxygen Biofuel Cell with a Substrate-Modified Biocathode. *Phys. Chem. Chem. Phys.* **2014**, *16* (10), 4823–4829. https://doi.org/10.1039/C3CP54888K
(56) Suzuki, Y.; Makino, F.; Miyata, T.; Tanaka, H.; Namba, K.; Kano, K.; Sowa, K.; Kitazumi, Y.; Shirai, O. Essential Insight of Direct Electron Transfer-Type Bioelectrocatalysis by Membrane-Bound D-Fructose Dehydrogenase with Structural Bioelectrochemistry. *ACS Catal.* **2023**, *13* (20), 13828–13837. https://doi.org/10.1021/acscatal.3c03769
(57) Hibino, Y.; Kawai, S.; Kitazumi, Y.; Shirai, O.; Kano, K. Mutation of Heme *c* Axial Ligands in D-Fructose Dehydrogenase for Investigation of Electron Transfer Pathways and Reduction of

Overpotential in Direct Electron Transfer-Type Bioelectrocatalysis. *Electrochem. Commun.* **2016**, *67*, 43–46. https://doi.org/10.1016/j.elecom.2016.03.013
(58) Hibino, Y.; Kawai, S.; Kitazumi, Y.; Shirai, O.; Kano, K. Construction of a Protein-Engineered Variant of D-Fructose Dehydrogenase for Direct Electron Transfer-Type Bioelectrocatalysis. *Electrochem. Commun.* **2017**, *77*, 112–115. https://doi.org/10.1016/j.elecom.2017.03.005
(59) Ikeda, T.; Kobayashi, D.; Matsushita, F. Bioelectrocatalysis at Electrodes Coated with Alcohol Dehydrogenase, a Quinohemoprotein with Heme *c* Serving as a Built-In Mediator. *J. Electroanal. Chem.* **1993**, *361* (1–2), 221–228. https://doi.org/10.1016/0022-0728(93)87058-4
(60) Tsujimura, S.; Abo, T.; Ano, Y.; Matsushita, K.; Kano, K. Electrochemistry of D-Gluconate 2-Dehydrogenase from *Gluconobacter frateurii* on Indium Tin Oxide Electrode Surface. *Chem. Lett.* **2007**, *36* (9), 1164–1165. https://doi.org/10.1246/cl.2007.1164
(61) Tkac, J.; Svitel, J.; Vostiar, I.; Navratil, M.; Gemeiner, P. Membrane-Bound Dehydrogenases from *Gluconobacter* sp.: Interfacial Electrochemistry and Direct Bioelectrocatalysis. *Bioelectrochemistry* **2009**, *76* (1–2), 53–62. https://doi.org/10.1016/j.bioelechem.2009.02.013
(62) Adachi, T.; Kitazumi, Y.; Shirai, O.; Kano, K. Direct Electron Transfer-Type Bioelectrocatalysis by Membrane-Bound Aldehyde Dehydrogenase from *Gluconobacter oxydans* and Cyanide Effects on Its Bioelectrocatalytic Properties. *Electrochem. Commun.* **2021**, *123*, 106911. https://doi.org/10.1016/j.elecom.2020.106911
(63) Sowa, K.; Okuda-Shimazaki, J.; Fukawa, E.; Sode, K. Direct Electron Transfer–Type Oxidoreductases for Biomedical Applications. *Annu. Rev. Biomed. Eng.* **2024**, *26*, 357–382. https://doi.org/10.1146/annurev-bioeng-110222-101926
(64) Prust, C.; Hoffmeister, M.; Liesegang, H.; Wiezer, A.; Fricke, W. F.; Ehrenreich, A.; Gottschalk, G.; Deppenmeier, U. Complete Genome Sequence of the Acetic Acid Bacterium *Gluconobacter oxydans*. *Nat. Biotechnol.* **2005**, *23*, 195–200. https://doi.org/10.1038/nbt1062
(65) Adachi, T.; Miyata, T.; Makino, F.; Tanaka, H.; Namba, K.; Kano, K.; Sowa, K.; Kitazumi, Y.; Shirai, O. Experimental and Theoretical Insights into Bienzymatic Cascade for Mediatorless Bioelectrochemical Ethanol Oxidation with Alcohol and Aldehyde Dehydrogenases. *ACS Catal.* **2023**, *13* (12), 7955–7965. https://doi.org/10.1021/acscatal.3c01962
(66) Gomi, M.; Akazawa, F.; Mitaku, S. SOSUIsignal: Software System for Prediction of Signal Peptide and Membrane Protein. *Genome Informatics* **2000**, *11*, 414–415. https://doi.org/10.11234/gi1990.11.414
(67) Sugimoto, Y.; Kawai, S.; Kitazumi, Y.; Shirai, O.; Kano, K. Function of C-Terminal Hydrophobic Region in Fructose Dehydrogenase. *Electrochim. Acta* **2015**, *176*, 976–981. https://doi.org/10.1016/j.electacta.2015.07.142
(68) Bollella, P.; Hibino, Y.; Kano, K.; Gorton, L.; Antiochia, R. Enhanced Direct Electron Transfer of Fructose Dehydrogenase Rationally Immobilized on a 2-Aminoanthracene Diazonium Cation Grafted Single-Walled Carbon Nanotube Based Electrode. *ACS Catal.* **2018**, *8* (11), 10279–10289. https://doi.org/10.1021/acscatal.8b02729
(69) Ichikawa, K.; Adachi, T.; Kitazumi, Y.; Shirai, O.; Sowa, K. Quantitative Elucidation of Catalytic Reaction of Truncated Aldehyde Dehydrogenase Based on Linear Free Energy Relationship. *ChemRxiv* **2024**. https://doi.org/10.26434/chemrxiv-2024-fb7hr
(70) Kawai, S.; Goda-Tsutsumi, M.; Yakushi, T.; Kano, K.; Matsushita, K. Heterologous Overexpression and Characterization of a Flavoprotein-Cytochrome c Complex Fructose Dehydrogenase of *Gluconobacter japonicus* NBRC3260. *Appl. Environ. Microbiol.* **2013**, *79* (5), 1654–1660. https://doi.org/10.1128/AEM.03152-12
(71) Ameyama, M.; Shinagawa, E.; Matsushita, K.; Adachi, O. D-Fructose Dehydrogenase of *Gluconobacter industrius*: Purification, Characterization, and Application to Enzymatic Microdetermination of D-Fructose. *J. Bacteriol.* **1981**, *145* (2), 814–823. https://doi.org/10.1128/jb.145.2.814-823.1981
(72) Mastronarde, D. N. Automated Electron Microscope Tomography Using Robust Prediction of Specimen Movements. *J. Struct. Biol.* **2005**, *152* (1), 36–51. https://doi.org/10.1016/j.jsb.2005.07.007
(73) Yonekura, K.; Maki-Yonekura, S.; Naitow, H.; Hamaguchi, T.; Takaba, K. Machine Learning-Based Real-Time Object Locator/Evaluator for Cryo-EM Data Collection. *Commun. Biol.* **2021**, *4*, 1044. https://doi.org/10.1038/s42003-021-02577-1.
(74) Carragher, B.; Cheng, Y.; Frost, A.; Glaeser, R. M.; Lander, G. C.; Nogales, E.; Wang, H.-W. Current Outcomes When Optimizing 'Standard' Sample Preparation for Single-Particle Cryo-EM. *J. Microsc.* **2019**, *276* (1), 39–45. https://doi.org/10.1111/jmi.12834
(75) Tsujimura, S.; Nakagawa, T.; Kano, K.; Ikeda, T. Kinetic Study of Direct Bioelectrocatalysis of Dioxygen Reduction with Bilirubin Oxidase at Carbon Electrodes. *Electrochemistry* **2004**, *72* (6), 437–439. https://doi.org/10.5796/electrochemistry.72.437
(76) Das, D. K.; Medhi, O. K. Effect of Surfactant and pH on the Redox Potential of Microperoxidase 11 in Aqueous Micellar Solutions. *J. Chem. Soc., Dalton Trans.* **1998**, (10), 1693–1698. https://doi.org/10.1039/A708732B